Cyclic metal plasticity model parameters with limited information: a constrained optimization approach

Albano de Castro e Sousa[1], Ph.D.

Alexander R. Hartloper [2], MEng, S.M ASCE

Dimitrios G. Lignos [3], Ph.D, M. ASCE

ABSTRACT

Tensile test data for structural steels are ubiquitous. Yet, the information monotonic loading provides with respect to the material's characteristics is limited. Notably, features of inelastic response to cyclic loading, such as the Bauschinger effect, can not be determined without testing with a load reversal protocol. This paper aims at addressing this shortcoming by formulating a constrained optimization problem that provides best-fit material parameters to a tensile test, while simultaneously imposing representative cyclic properties for structural steels. Recommendations on constraints are given. Results demonstrate that improvements can be achieved when compared to: (1) direct fits to tensile data and (2) input model parameters from the same steel material but from different batches calibrated to a wide range of strain-based protocols. Given the available data, it is concluded that simpler models with one backstress tend to perform best with the proposed constraints.

Keywords: Inverse problem, structural steel, tensile test, material constitutive modeling, Earthquake loading, cyclic hardening, constrained optimization

INTRODUCTION

[1]Post-Doctoral Researcher, École Polytechnique Fédérale de Lausanne. EPFL ENAC IIC RESSLab, GC B3 465, Station 18, 1015 Lausanne, Switzerland. E-mail: albano.sousa@epfl.ch

[2]Doctoral Assistant, École Polytechnique Fédérale de Lausanne. EPFL ENAC IIC RESSLab, GC B3 514, Station 18, 1015 Lausanne, Switzerland. E-mail: alexander.hartloper@epfl.ch

[3]Associate Professor, École Polytechnique Fédérale de Lausanne. EPFL ENAC IIC RESSLab, GC B3 485, Station 18, 1015 Lausanne, Switzerland.(corresponding author). E-mail: dimitrios.lignos@epfl.ch

Seismic response of steel structures to extreme events is often nonlinear in nature. The sources of the nonlinearity can be classified mainly into two categories: (1) material and (2) geometric. Without accurate material and geometric properties, reliable physics-based modeling of the hysteretic response of a component or sub-assembly can not be established. Consequently, their impact at the system level can be the source of accumulated errors that may lead to misleading conclusions of overall structural performance. Yet, all too often are structural steel's nonlinearities oversimplified or all together overlooked. In situations where material and geometric nonlinearities strongly interact (*e.g.* open-section beam-columns), it has been shown that such oversimplifications can lead to distinct member failure modes (Hartloper et al. 2019a).

Accurate material modeling depends both on the constitutive model and on the ability to obtain its characteristic input parameters. Solving inverse problems, however, are marred with nonuniqueness issues (Cooke and Kanvinde 2015), *i.e.* a different set of parameters can yield the same overall material response for a particular loading history– *c.f. e.g.* Fig. 1. This feature can significantly hamper modeling efforts in situations where loading histories differ from the calibrated cases. For earthquake applications this is naturally an issue of concern due to the stochastic character of seismic action. To mitigate this problem, a methodology has been proposed to calibrate parameters to a rich set of protocols that are representative of seismic loading (de Castro e Sousa et al. 2020). While this approach shows promise, obtaining test data can be challenging since it can be costly both in terms of the number of specimens and of specialized testing equipment in order to achieve high compressive strains. Furthermore, there are situations, like the performance assessment of existing steel structures (CEN 2005; ASCE 2017), where collecting the required amount of samples may be challenging. Given that there is a need for accurate material modeling, on one hand, and that the ability to carry out extensive testing campaigns may be restricted, on the other hand, a way to use limited test information, such as monotonic tensile tests, is of particular interest to the research and practice communities.

Most of steel's mechanical design characteristics are typically obtained by tensile tests. These tests are both common and standardized (ASTM 2013; CEN 2001), meaning they are relatively economical and the testing methodology is established. Their main shortcoming, however, is that they can not depict how the material would behave under cyclic loading. Importantly, the extent of the Bauschinger effect and isotropic versus kinematic hardening saturation levels are information that cannot be derived solely from monotonic loading. This paper proposes addressing this challenge by determining material parameters from a specific tensile test but that, at the same time, satisfy some *a priori* knowledge pertaining to its cyclic properties. It is envisioned that this *a priori* knowledge should be directly related to the steel grades' general material characteristics, *e.g.* its microstructure (in its grain size and crystalline structure) or its chemical composition. As will be shown more concretely in the methodology and results sections, different steel grades commonly present different ratios of isotropic to kinematic hardening, a behavior believed to be closely related to the material's grain refinement (Bouaziz et al. 2008).

The interpretation of material parameters is inextricably tied to the chosen model representation. Herein, two materials models are used: (1) the Voce-Chaboche (VC) (Voce 1948; Chaboche et al. 1979) and (2) an Updated Voce-Chaboche (UVC) (Hartloper et al. 2020). Both are part of the rate independent, J_2 plasticity framework, but differ on their hardening rules - the isotropic, in particular. The first is a widely used material model in the context of nonlinear analysis of steel structures (*c.f.* *e.g.* Fell et al. (2009), Araújo et al. (2017), Elkady and Lignos (2018)). Among its most important features is its ability to adequately capture cyclic loading behavior with exponentially saturating hardening laws. The second builds upon the VC by adjusting the material response to more accurately capture the discontinuous yielding phenomenon present in mild steels (Lubliner 2008). Both models aim at representing physical mechanisms that lead to work hardening - *e.g.* the Bauschinger effect through the kinematic hardening representation. However, the interpretation of material parameters through these models should only be made if they can be determined in a reliable

and consistent manner.

The approaches made in de Castro e Sousa et al. (2020) and Hartloper et al. (2019b) are focused toward consistency of the parameters obtained for the VC and UVC models, respectively. Therein, unconstrained optimization procedures, based on Newton Trust-Region (NTR) framework, are presented that are able to navigate the non-convex parameter search space both efficiently and reliably, given a diverse set of strain-based load protocols. The parameters obtained for each of these models, with those methodologies, are considered to be intrinsic to the material since they are both reliable and physically motivated. While differences between steel production batches are to be expected, the hypothesis is made that certain behavioral aspects are directly transferable between materials of the same grade; that is to say that, specific material parameters might be different but, for example, ratios of isotropic to kinematic hardening should remain largely of the same magnitude for a given steel grade.

This paper concerns itself with answering mainly one question: can parameter optimization of a single tensile test, holding constant characteristic material ratios for cyclic loading, return satisfactory stress-strain responses for a wide range of cyclic load protocols? There is a pressing need for an answer to this question. Consider, for example, Fig. 1 which depicts test results for two load protocols (Fig. 1a /1c- monotonic; Fig. 1b/1d - cyclic variable amplitude)[1]. On top of the test results, two uniaxial VC model responses for the tests' strain histories are also depicted, whose parameters are determined with (1) a wide range of cyclic load protocols and (2) naively with only the tensile test data. It can be seen that, although the parameters perform similarly in the tensile case, the tensile fitting's response deviates largely from the variable amplitude response. Naive tensile-only calibrations do not perform well when simulating cyclic loading because monotonic tensile tests do not contain information regarding the Bauschinger effect nor cyclic hardening, therefore, it can be taken for granted that naively using a tensile test to calibrate a cyclic material model is an inad-

[1]load protocol designations can be consulted in de Castro e Sousa et al. (2020)

equate approach. Since it has been shown that even small differences in a material model can have a disproportionate effect on the overall member behavior and influence simulated geometric instabilities (Hartloper et al. 2019a), this aspect may be crucial in the accuracy of structural responses in the nonlinear regime.

To address the problem stated above, an approach is proposed in this paper that makes use of (1) material performance metrics and (2) a constrained optimization procedure using the developed metrics in order to solve for the corresponding model parameters . Their efficacy is evaluated by using appropriate error metrics. Additionally, comparisons are made to material model performance using parameters from known databases for nominally identical materials. It is shown that the proposed method outperforms a "naive" optimization, and is on-or-above par with the use of relevant parameters from databases, for the case-study addressed herein. Details for the approach are given in the Methodology section. After, results of the application of the methodology to a number of materials are presented and a discussion of those results is given in the subsequent section. The paper concludes with a brief section summarizing the main outcomes of this research.

METHODOLOGY

A solution to the problem of determining a set of constitutive model parameters representative for cyclic loading using only a tensile test is proposed in this section. The workflow of the proposed methodology is shown in Fig. 2 applied to structural steel materials. The workflow consists of three stages for a given steel material: Stage 1: determine the *a priori* cyclic hardening characteristics of the material for a set constitutive model, Stage 2: use this *a priori* information to inform the model calibration using only a tensile test, and Stage 3: validate the results.

In Stage 1, the metrics to quantify the behavior of steel materials subjected to cyclic loading, and the associated constraints, are proposed. An existing database of uniaxial cyclic tests, denoted as the Root dataset, is used to calculate the bounds in these constraints for selected materials through established calibration methods (Hartloper et al. 2019b; de

Castro e Sousa et al. 2020). In Stage 2, the constraints are used with tensile tests to form a constrained optimization problem using this limited data. The solution to this minimization problem yields the constitutive model parameters that match a tensile test with cyclic loading information embedded. In Stage 3, an assessment of the methodology is made by comparing the predicted steel material response using the tensile-only parameters with uniaxial coupon tests from the Root dataset in addition to a separate dataset (denoted the Validation dataset) to avoid bias in the results.

Database of Steel Materials

As shown in Fig. 2, data regarding the cyclic and tensile behavior of steel materials is required at each step of the process, therefore, a database of such information is a necessary starting point. An existing database of uniaxial tensile tests on structural steel materials, in combination with several uniaxial cyclic tests conducted on round-bar coupons, is utilized in this paper (Grigoriou and Lignos 2017; Suzuki 2018; Hartloper et al. 2020). This database contains the original data used in the authors' research in the domain of inverse problems and is thus coined the Root dataset. A further description of the database, including the definitions of the cyclic load protocols used, is provided in de Castro e Sousa et al. (2020). In brief, the strain-based load protocols are cataloged numerically into 10 different histories that are deemed to be representative of strain histories in steel frame structural components when subjected to earthquake loading. In total, nine sets of different steel materials (some materials having multiple samples) are included in the database, as summarized Table 1.

The Root dataset (Table 1) is largely comprised of low-carbon (or mild) low-alloy structural steels that are commonly used in Europe (*e.g.* S355J2 and S355J2+N), North America (*e.g.* A992 Gr. 50 and A500 Gr. B), and Japan (*e.g.* BCR295 and BCP325) (CEN 2005; ASTM 2016; ASTM 2018). These mild steel materials are the focus of this study. Other materials included in Table 1 are high-strength low-alloy steels (S460NL and S690QL) (CEN 2019b; CEN 2019a), and a high-performance steel that is manufactured with a thermomechanically controlled process and grain refinement (HYP400) (Suzuki et al. 2008) that are

of emerging interest in structural earthquake engineering. However, only a single set of tests is available for each of these materials, and therefore, the hardening characteristics of these materials cannot be reliably established at this time. Informative results for these materials are included for use in future work that may expand on the present study.

Definition of the Constitutive Models

Implementation of the VC and UVC models has already been extensively described in the literature (Hartloper et al. 2019b; de Castro e Sousa et al. 2020), therefore, only pertinent details are covered herein for brevity. The model implementation outlined in this section is specific to uniaxial stress states owing to the nature of the data included in the previously described database.

Both the VC and UVC models use a von Mises yield condition, ϕ^{VM},

$$\phi^{VM} := |\sigma - \alpha| - (\sigma_{y,0} + K) \leq 0, \tag{1}$$

where σ is the uniaxial stress, α is the backstress defining the kinematic hardening component, $\sigma_{y,0}$ is the initial yield stress, and K is the isotropic hardening. The isotropic hardening rule defined in the UVC model is

$$K = Q_\infty \left(1 - \exp\left[-b\varepsilon^p_{eq}\right]\right) - D_\infty \left(1 - \exp\left[-a\varepsilon^p_{eq}\right]\right), \tag{2}$$

where $\dot{\varepsilon}^p_{eq} = |\dot{\varepsilon}^p|$ is the equivalent plastic strain, Q_∞ is the magnitude of isotropic hardening at model saturation, b is the associated rate parameter, D_∞ and a are parameters to account for discontinuous yielding in structural steels. The over-dot indicates the derivative with respect to time. The parameter D_∞ imposes an initial reduction in the yield surface that saturates quickly when the rate parameter a is properly chosen. Isotropic hardening in the classic VC model is attributed to Voce (1948), and is simply recovered by removing the D_∞ term from Eqn. 2. Removal of this term is the only difference in the hardening rules between the VC and UVC models.

Both material models employ the nonlinear kinematic hardening rule proposed by Chaboche et al. (1979) based on the work of Armstrong and Fredrick (1966). The Chaboche hardening rule is $\alpha = \sum_k^{N_k} \alpha_k$, where α_k are backstress components, $k = 1, 2, \ldots, N_k$. Each component is defined by the Armstrong-Frederick rule for uniaxial loading,

$$\dot{\alpha}_k = \text{sign}\left[\sigma - \alpha\right] C_k \dot{\varepsilon}^p_{eq} - \gamma_k \alpha_k \dot{\varepsilon}^p_{eq}, \tag{3}$$

where C_k is the magnitude of contribution to the total backstress for component k, and γ_k is the corresponding rate parameter. In this paper, the backstress rate parameters are defined such that $\gamma_1 > \gamma_2 > \cdots > \gamma_{N_k}$.

Two constraints on the set of UVC parameters are required for modeling structural steels (Hartloper et al. 2019b); they are denoted g_1 and g_2, and are respectively defined as

$$g_1 := -Q_\infty b - \sum_k C_k + D_\infty a \leq 0, \tag{4}$$

$$g_2 := Q_\infty b^2 + \sum_k C_k \gamma_k - D_\infty a^2 \leq 0. \tag{5}$$

These two constraints are sufficient conditions for the set of UVC model parameters to lead to a non-softening stress-strain response, therefore, they are considered an essential component of the UVC model for structural steels. Constraints (4) and (5) do not apply to the VC model.

Considering the uniaxial stress state, the addition of the elastic modulus, E, completes the set of parameters. The set of parameters for the VC and UVC models are respectively

$$\boldsymbol{x}^{VC} = \left[E, \sigma_{y,0}, Q_\infty, b, C_1, \gamma_1, \ldots, C_{N_k}, \gamma_{N_k}\right],$$

and

$$\boldsymbol{x}^{UVC} = \left[E, \sigma_{y,0}, Q_\infty, b, D_\infty, a, C_1, \gamma_1, \ldots, C_{N_k}, \gamma_{N_k}\right].$$

Definition of the Inverse Problem

Following de Castro e Sousa et al. (2020), an objective function is defined that represents the error in the model prediction based on the squared strain energy. The objective function $f(\boldsymbol{x}) : \mathbb{R}^n \to \mathbb{R}$ is

$$f(\boldsymbol{x}) = \sum_{j=1}^{N_T} \frac{\int_0^{\varepsilon_j^*} \left(\sigma_j^{model}\left(\varepsilon_j; \boldsymbol{x}\right) - \sigma_j^{test}\right)^2 \mathrm{d}\epsilon^*}{\int_0^{\varepsilon_j^*} \mathrm{d}\epsilon^*}, \tag{6}$$

where $\sigma_j^{model}\left(\varepsilon_j; \boldsymbol{x}\right)$ is the predicted model stress given a strain history ε_j and parameters $\boldsymbol{x}$, σ_j^{test} is the stress recorded in the uniaxial test j, and ε^* is the accumulated strain

$$\varepsilon_j^* = \int_0^{t_j} |\dot{\varepsilon}_j| \mathrm{d}\tau. \tag{7}$$

Note that Eqn. 6 is defined for N_T load histories allowing for multiple cyclic tests to be used in the calibration simultaneously.

We seek the set of parameters that minimizes the defined objective function, *i.e.*, the inverse problem of parameter calibration is posed as the constrained minimization problem

$$\underset{\boldsymbol{x} \in \mathbb{R}^n}{\text{minimize}} \quad f(\boldsymbol{x}) \tag{8a}$$

$$\text{subject to} \quad \boldsymbol{g}(\boldsymbol{x}) \leq \boldsymbol{0}, \tag{8b}$$

where $\boldsymbol{g}(\boldsymbol{x}) : \mathbb{R}^n \to \mathbb{R}^m$ is a vector valued function of m constraints given n parameters in $\boldsymbol{x}$. These constraints are an essential component of the proposed methodology as they embed characteristics of the material subjected to cyclic loading into just a single tensile test.

Definition of the Constraints to Embed Cyclic Loading Information

Metrics are proposed to characterize the behavior of structural steels subjected to cyclic loading. These metrics should be derived from tests that are representative of the expected loading conditions of the material. In the context of the current paper, the load protocols should be consistent with the expected inelastic strain demands in steel components under

earthquake loading. Constraints on these metrics are then defined to embed this information into the calibration process when only a tensile test is used.

Material Hardening Metrics

The metrics defined herein are consistent with those used in de Castro e Sousa et al. (2020) to quantify the isotropic and kinematic hardening found in structural steels. Given a set of parameters for either the UVC or VC models, the following metrics are defined in terms of the equivalent plastic strain assuming monotonic loading from an initially strain free state. This assumption is necessary to define metrics independent of the strain history for the kinematic hardening component because the time-integration of Eqn. 3 is not a monotonically increasing function under cyclic loading. Where applicable, the metrics for the VC model are calculated neglecting D_∞ and a.

The total increase in stress due to combined isotropic and kinematic hardening is described by the metric

$$\sigma_{hard}\left(\varepsilon_{eq}^{p}\right) = Q_\infty\left(1-\exp\left[-b\varepsilon_{eq}^{p}\right]\right) + \sum_k C_k/\gamma_k\left(1-\exp\left[-\gamma_k\varepsilon_{eq}^{p}\right]\right), \tag{9}$$

and the ratio of isotropic-to-total hardening is defined by the metric

$$\rho_{iso}\left(\varepsilon_{eq}^{p}\right) = \frac{Q_\infty\left(1-\exp\left[-b\varepsilon_{eq}^{p}\right]\right)}{\sigma_{hard}\left(\varepsilon_{eq}^{p}\right)}. \tag{10}$$

A value of $\rho_{iso} = 1$ indicates that there is only isotropic hardening present in the material, and $\rho_{iso} = 0$ indicates purely kinematic hardening (*e.g.*, in high-strength steels). The total stress at a particular value of ε_{eq}^{p} is defined by

$$\sigma_{total}\left(\varepsilon_{eq}^{p}\right) = \sigma_{y,0} + \sigma_{hard}\left(\varepsilon_{eq}^{p}\right) - D_\infty\left(1-\exp\left[-a\varepsilon_{eq}^{p}\right]\right), \tag{11}$$

and the ratio of total stress to the initial yield stress is defined as

$$\rho_{yield}\left(\varepsilon^p_{eq}\right) = \frac{\sigma_{total}\left(\varepsilon^p_{eq}\right)}{\sigma_{y,0}}. \tag{12}$$

A value of $\rho_{yield} = 2$ would indicate that the stress at the chosen value of ε^p_{eq} is twice the initial yield stress. In this paper, all the metrics are defined at their saturation value, $\varepsilon^p_{eq} \to \infty$, this is indicated by the *sat* superscript, *e.g.*, $\rho^{sat}_{iso} = Q_\infty/\left(Q_\infty + \sum_k C_k/\gamma_k\right)$.

A further metric is introduced relating the rates of kinematic and isotropic hardening. This metric quantifies the rates at which the different hardening components saturate assuming monotonic loading, and is defined as

$$\rho_{\gamma_1 b} = \frac{\gamma_1}{b}. \tag{13}$$

If $\rho_{\gamma_1 b} > 1$ this indicates that the kinematic hardening saturates at a lower equivalent plastic strain than the isotropic hardening under monotonic loading. A metric is proposed to define the rate of saturation for various kinematic hardening components if more than one backstress is specified in the constitutive model:

$$\rho_{\gamma_1 \gamma_2} = \frac{\gamma_1}{\gamma_2}. \tag{14}$$

This constraint is necessary to prevent duplication of the backstress rate terms, for instance, if $\gamma_1 = \gamma_2$, then essentially the two-backstress model reduces to a one-backstress model. This issue arises because there is not enough information in a single tension test to differentiate the kinematic hardening components since a near-perfect fit can be obtained with a single component (see Figs. 1a and 1c). Whereas, this same issue only appears to occur after four backstresses are included when the full set of load protocols are used in the calibration effort (de Castro e Sousa et al. 2020).

An additional metric is proposed for the UVC model that specifies the ratio of the initial

reduction in the yield surface to the total hardening at saturation. More specifically,

$$\rho_D\left(\varepsilon_{eq}^p\right) = \frac{D_\infty\left(1-\exp\left[-a\varepsilon_{eq}^p\right]\right)}{Q_\infty\left(1-\exp\left[-b\varepsilon_{eq}^p\right]\right)+\sum_k C_k/\gamma_k\left(1-\exp\left[-\gamma_k\varepsilon_{eq}^p\right]\right)}. \tag{15}$$

Another possible constraint is to specify the ratio between D_∞ and Q_∞, however, this constraint is not valid for steels with very low isotropic hardening (*e.g.*, high strength steels). This is also common in the case of cold-forming, such as in the corners of press-bent products.

Constraints on the Hardening Metrics

Constraints are imposed on each of the metrics described in the previous section for use in the constrained minimization problem. All the constraints are posed as bound constraints in the standard form specified in (8b), therefore, two constraints are defined for the lower and upper bound of each metric, g^{inf} and g^{sup}, respectively. Each of the following constraints consists of a metric, ρ, and a constant that specifies the lower/upper bound of the metric, $c^{inf/sup}$.

In total, there are ten constraints specified assuming a maximum of two backstresses in the constitutive model:

$$g_{yield}^{inf} := c_{yield}^{inf} - \rho_{yield}^{sat}; \quad g_{yield}^{sup} := \rho_{yield}^{sat} - c_{yield}^{sup}; \tag{16a}$$

$$g_{iso}^{inf} := c_{iso}^{inf} - \rho_{iso}^{sat}; \quad g_{iso}^{sup} := \rho_{iso}^{sat} - c_{iso}^{sup}; \tag{16b}$$

$$g_{\gamma_1 b}^{inf} := c_{\gamma_1 b}^{inf} - \rho_{\gamma_1 b}; \quad g_{\gamma_1 b}^{sup} := \rho_{\gamma_1 b} - c_{\gamma_1 b}^{sup}; \tag{16c}$$

$$g_{\gamma_1\gamma_2}^{inf} := c_{\gamma_1\gamma_2}^{inf} - \rho_{\gamma_1\gamma_2}; \quad g_{\gamma_1\gamma_2}^{sup} := \rho_{\gamma_1\gamma_2} - c_{\gamma_1\gamma_2}^{sup}; \tag{16d}$$

$$g_{D}^{inf} := c_{D}^{inf} - \rho_{D}^{sat}; \quad g_{D}^{sup} := \rho_{D}^{sat} - c_{D}^{sup}; \tag{16e}$$

The constants in each of (16a)–(16e) depend on the constitutive model (*e.g.,* VC or UVC, including the number of backstresses assumed), and the equivalent plastic strain used in computing the corresponding metrics (*e.g.,* at saturation). Both these factors should be consistent with the calibration at hand when computing the constants.

Proposed Calibration Procedure

The optimization problem (8a) subjected to (8b) is solved with the NITRO algorithm (Byrd et al. 1999) as implemented in Scipy (Virtanen et al. 2020). The NITRO algorithm requires an initial starting point, and is an iterative method where the stopping point for a local minimum is determined by the first- and second-order necessary conditions (i.e., the norm of the objective function's gradient is less than a specified tolerance, and the objective function's Hessian is positive definite). Gradients and Hessians required in this algorithm are computed using algorithmic differentiation, as previous studies have demonstrated the efficacy of this approach when combined with gradient-based optimization methods (Hartloper et al. 2019b; de Castro e Sousa et al. 2020).

The use of a minimization algorithm requires an initial starting point. Two starting points are used in this study to assess if similar optimal parameters are obtained from different initial conditions. The first starting point, denoted as SP1, is feasible with respect to the constraint set. To generate SP1, an initial set of parameters is chosen that represents an elastic perfectly-plastic material as assumed in de Castro e Sousa et al. (2020); this set is then modified according to Algorithm 1 so that the initial point is feasible with respect to the constraints. The basis for this algorithm is to set the parameters such that the constraints are set to their mean of the upper and lower bound values. The second starting point, SP2, is a potentially infeasible point that is just the set of parameters leading to a nearly perfectly-plastic response (SP1 prior to applying Algorithm 1).

With reference to Stage 2 of the workflow shown in Fig. 2, the proposed procedure for calibration of the VC and UVC model parameters using only a tensile test is as follows:

1. **Specify the constraints:**

   (a) VC model: The constraint vector, $g(x)$, is composed of constraints (16a)–(16c) regardless of the model and number of backstresses. Constraints defined in (16d) are added if two backstresses are considered.

(b) UVC model: The constraint vector, $g(x)$, is composed in the same manner as the VC model for either one or two backstresses. Additionally, g_1 and g_2 are added to ensure non-softening of the material.

2. **Set the material cyclic hardening metric constraint bounds:** The bounds on the constraints are defined using the minima and maxima of relevant metrics from prior calibrations on similar materials using relevant cyclic loading histories. The metrics used to establish the bounds should match the employed material model and number of backstresses for the constraints to be meaningful.

   (a) VC model:

   - One backstress: c_{yield}^{inf}, c_{yield}^{sup}, c_{iso}^{inf}, c_{iso}^{sup}, $c_{\gamma_1 b}^{inf}$, $c_{\gamma_1 b}^{sup}$,
   - Two backstresses: VC model one backstress, additionally $c_{\gamma_1\gamma_2}^{inf}$, $c_{\gamma_1\gamma_2}^{sup}$

   (b) UVC model:

   - One backstress: VC model one backstress, additionally c_D^{inf}, c_D^{sup}
   - Two backstresses: VC model two backstresses, additionally c_D^{inf}, c_D^{sup}

3. **Select the starting point:** The starting point is intended to represent a material with nominal elastic and yield properties, and a nearly-perfectly plastic behavior. Nominal values for the elastic modulus and yield stress are selected as $E_n = 200$ GPa and $f_{y,n} = 355$ MPa for all materials in this study.

   (a) VC model:

   - One backstress: $x_{SP2}^{VC} = [E_n, f_{y,n}, 1, 1, 1, 1]$
   - Two backstresses: $x_{SP2}^{VC} = [E_n, f_{y,n}, 1, 1, 1, 1, 1, 1]$

   (b) UVC model: Note that the initial value for "a" is set to 200 to approximately reach 99 % saturation of D_∞ at 2 % strain (typical plateau strain in mild steels).

   - One backstress: $x_{SP2}^{UVC} = [E_n, f_{y,n}, 1, 1, 1, 200, 1, 1]$

- Two backstresses: $x_{SP2}^{UVC} = [E_n, f_{y,n}, 1, 1, 1, 200, 1, 1, 1, 1]$

4. **(Optional) Make the starting point feasible:** If desired, Algorithm 1 can be applied to x_{SP2}^{VC} / x_{SP2}^{UVC} so that the starting point satisfies the hardening metric constraint bounds. The basis of this algorithm is to set the material properties to the average of the relevant bounds. The feasible starting point is denoted x_{SP1}^{VC} / x_{SP1}^{UVC}.

5. **Determine the optimal set of parameters:** The minimization, Problem (8), is solved using the NITRO algorithm starting from SP1 or SP2 with a tolerance on the convergence criteria of 10^{-8} and a maximum of 600 iterations. Note that the solution point typically converges to a local minima within 200 iterations for the steel materials examined in this paper (on average, approximately 5 minutes on a desktop computer with a 4 GHz processor), therefore, the 600 iterations is deemed to be adequate.

Algorithm 1 Generate a feasible starting point with respect to g_{yield}, g_{iso}, $g_{\gamma_1 b}$, $g_{\gamma_1\gamma_2}$.

$\rho_{yield,avg}^{sat} \leftarrow 0.5 \times \left(c_{yield}^{inf} + c_{yield}^{sup}\right)$
$\rho_{iso,avg}^{sat} \leftarrow 0.5 \times \left(c_{iso}^{inf} + c_{iso}^{sup}\right)$
$\rho_{\gamma_1 b,avg}^{sat} \leftarrow 0.5 \times \left(c_{\gamma_1 b}^{inf} + c_{\gamma_1 b}^{sup}\right)$
$\rho_{\gamma_1\gamma_2,avg} \leftarrow 0.5 \times \left(c_{\gamma_1\gamma_2}^{inf} + c_{\gamma_1\gamma_2}^{sup}\right)$
$\gamma_{2,0} \leftarrow \gamma_{1,0}/\rho_{\gamma_1\gamma_2,avg}$
$C_{1,0} \leftarrow -\gamma_{1,0}\sigma_{y,0,0}\left(-1+\rho_{iso,avg}\right)\left(-1+\rho_{yield,avg}\right)$
$Q_{\infty,0} \leftarrow C_{1,0}\rho_{iso,avg}/\left(\gamma_{1,0}\left(-1+\rho_{iso,avg}\right)\right)$
$b_0 \leftarrow \gamma_{1,0}/\rho_{\gamma b,avg}$

Metrics Used for Procedure Evaluation

Referring to Stage 3 of the proposed workflow shown in Fig. 2, the normalized form of the objective function is used to assess the accuracy of the proposed calibration procedure using only a tensile test. The normalized error metric is

$$\bar{\varphi} = \sqrt{\frac{f(\boldsymbol{x})}{E_{total}}}, \tag{17}$$

where the total normalized strain energy of all the considered tests in a data set is

$$E_{total} = \sum_{j=1}^{N_T} \frac{\int_0^{\varepsilon_j^*} \left(\sigma_j^{test}\right)^2 \mathrm{d}\epsilon^*}{\int_0^{\varepsilon_j^*} \mathrm{d}\epsilon^*}. \tag{18}$$

The metric $\bar{\varphi}$ represents the error in strain energy calculated over the entire data set (*i.e.,* tensile and cyclic tests), normalized by the total strain energy of all the tests.

Consistency between sets of parameters is evaluated using the ξ_2 metric defined in de Castro e Sousa et al. (2020). This metric is computed between two sets of parameters $\boldsymbol{x}_{base}$ and $\boldsymbol{x}_{sample}$ as

$$\xi_2 = \frac{\left(\boldsymbol{x}_{sample} - \boldsymbol{x}_{base}\right)^T \boldsymbol{\nabla}_{xx} f(\boldsymbol{x}_{base}) \left(\boldsymbol{x}_{sample} - \boldsymbol{x}_{base}\right)}{E_{total}}, \tag{19}$$

where $\boldsymbol{\nabla}_{xx} f(\boldsymbol{x}_{base})$ is the Hessian of the objective function for a given data set evaluated at the local minimum of $f(\boldsymbol{x})$, $\boldsymbol{x}_{base}$. The ξ_2 metric represents the normalized increase in the minimum value of the objective function when choosing $\boldsymbol{x}_{sample}$ instead of $\boldsymbol{x}_{base}$. If this increase is insignificant, then the two sets of parameters are said to be consistent.

Validation of the Results

The main objective of this paper is to answer the question of whether calibrations of single tensile tests, constrained by cyclic material characteristics, will yield *satisfactory* responses for a wide range of cyclic protocols. Here, the proposed tensile-only calibration procedure is satisfactory if the results out-perform, in the $\bar{\varphi}$-sense for all LPs, parameters derived for other materials using all available load protocols. The satisfactory condition defined above reflects the common situation where a modeler selects input model parameters from a nominally identical steel grade that have been calibrated in a prior study for an entirely different production batch. For instance, parameters from de Castro e Sousa et al. (2020) for a hot-rolled HEB500 section of S355J2 ($f_y = 355$ MPa) steel may be selected to model an IPE300 section from a different production heat of the same steel grade. In this hypothetical situation, we would like to demonstrate that, on average, there is less error in the $\bar{\varphi}$-sense by using the proposed tensile-only calibration with a supplied tensile test than using alternative

parameters from the same steel grade.

Since the cyclic characteristics are obtained *a priori*, validation of the proposed methodology is done using data sets of S355J2 steel that are separate from the database summarized in Table 1 to avoid bias in the results. The characteristics are derived from the Root dataset (see Fig. 2) and used to analyze steel materials from another set, coined the Validation dataset. The Validation dataset consists of tests conducted on round-bar coupons of S355J2 steel (with same group of ten uniaxial cyclic load protocols) sampled from two alternative sources: (1) the web of an IPE300 hot rolled profile and (2) the flange of the same IPE300. The proposed calibration procedure described above is subsequently applied to estimate the model parameters using a single tensile test. Comparisons are then made to parameters that would be obtained if all available load protocols were used, as well as using the parameters from Tables 2 and 6 for S355 steels calibrated from the Root dataset.

RESULTS

The methodology proposed in the previous section is applied to the database of steel materials summarized in Table 1. Results for the VC material model are presented first, followed by the UVC model. In all cases, discussion of the results is delayed to the Discussion section.

Voce-Chaboche Model Results

Constraint Bounds

Bounds on the metrics used to form the constraints defined in (16a)–(16d), *i.e.*, the c values, are calculated using the parameters obtained for mild structural steels. As mentioned in the Methodology section, only the S355J2(+N), A992 Gr. 50, and BCP325 steels are utilized for the tensile-only calibration because these materials are consistent in terms of their nominal chemical compositions and yield/tensile stresses (see Table 1) (CEN 2005; ASTM 2016). The other materials included in Table 1 are excluded from the metric bounds, and the tensile-only calibration is not conducted. The materials are excluded on the basis that: (1) they are high-strength low-alloy steels (*e.g.*, S460NL and S690QL), (2) are cold

worked from the corners of hollow structural sections (*e.g.*, A500 Gr. B and BCR295), or (3) were manufactured with a thermomechanically controlled process and grain refinement (*e.g.*, HYP400). However, parameters and hardening metrics using all available protocols are provided for each material in the Root dataset for use in future research.

Parameters for the VC model with one and two backstresses computed using the methodology in de Castro e Sousa et al. (2020) are recorded for all the Root materials in Table 2. The material hardening metrics computed for the subset of mild steels are summarized in Table 3, and a summary of the metrics can be viewed graphically in Fig. 3. Most importantly, observe that the computed metrics in Table 3 depend on the number of backstresses included in the model, therefore, a separate set of bounds are used for either one or two backstresses. Notice that there is an increase in the ratio of kinematic hardening when two backstresses are included in the model, this is because the kinematic hardening is more accurately represented by two backstress components, thus increasing its relevance and magnitude. The total hardening, σ_{total}^{sat}, is also greater when two backstresses are included. The reason for this is that γ_1 in the one-backstress model is greater than γ_2 in the two-backstress model, therefore, the two-backstress model saturates at a much greater plastic strain than the one-backstress model. This issue could be addressed by evaluating this metric at a finite equivalent plastic strain value, but for simplicity, this is not taken into account herein. As for the initial yield stress, comparing the $\sigma_{y,0}$ values in Table 2 with the nominal yield stresses in Table 1, the VC model values are close to, but consistently lower than, the nominal yield stress values. This is a known issue with the VC model for structural steels, and is the motivation behind the development of the UVC model (Hartloper et al. 2019b).

Low coefficient of variation (CoV) values for the metrics imply consistency across the steel materials, thereby providing an indication of the link between the physical material properties and the proposed hardening metrics. Results in Fig. 3 suggest that a reasonably low variance in all metrics is found for the VC one-backstress model, while this variance is significantly larger for the ρ_{yield}^{sat} and $\rho_{\gamma_1 b}$ metrics of the two-backstress model. Furthermore,

the metric $\rho_{\gamma_1\gamma_2}$ applicable to the VC two-backstress model does not appear to be reliable given that the CoV is slightly lower than 90 %. Recall, however, that this constraint should be considered to avoid duplication of the γ_k parameters when two backstresses are used in the tensile-only calibration.

The constraint bounds applicable to mild steels contain the minima and maxima of the metrics in Table 3 for S355J2(+N), A992 Gr. 50, and BCP325 steels. For the VC one-backstress model, these bounds are: $1.5 \leq \rho_{yield}^{sat} \leq 2.5$, $0.35 \leq \rho_{iso}^{sat} \leq 0.50$, and $2.25 \leq \rho_{\gamma_1 b} \leq 3.25$. Similarly, the bounds used in this study for the VC model and two backstresses are: $1.75 \leq \rho_{yield}^{sat} \leq 2.3$, $0.15 \leq \rho_{iso}^{sat} \leq 0.30$, $8.5 \leq \rho_{\gamma_1 b} \leq 25.0$, and $13 \leq \rho_{\gamma_1\gamma_2} \leq 92$.

Tensile-Only Calibration Results

Bounds on the metrics are used to establish the constraint vector $\boldsymbol{g}(\boldsymbol{x})$ used in the proposed calibration procedure (Stage 2, Fig. 2) for the subset of *Root* data. Results for the tensile-only calibration of the seven selected steel materials are provided in Table 4. The normalized error metric values, $\bar{\varphi}$, in Table 4 are evaluated using the parameters in this table along with all the available load protocols for each steel material. Similarly, the values of the ξ_2 metric are calculated using Eqn. 19 with $\boldsymbol{x}_{base}$ taken from Table 2 for the full data calibration (the base), and $\boldsymbol{x}_{sample}$ taken from Table 4 for the tensile-only calibration (the sample). The results in Table 4 suggest that there is no benefit in this approach to use two versus only one backstress in terms of the value of the error function—in fact it is worse to use two backstresses. Also, if one takes the threshold value of $\xi_2 = 5$ % discussed in de Castro e Sousa et al. (2020), these results show that the tensile only parameters are inconsistent with those retrieved from a calibration a full set of load protocols. The implications of these findings are further expounded in the Discussion section.

The influence of the two starting points is shown in Fig. 4 for the S355J2+N 50 mm plate data set, and similar results hold for the other data sets although they are not shown herein. The convergence criteria at each iteration of the NITRO algorithm is shown in Fig. 4a, and the results imply that the starting point does not have a major influence on the rate of

convergence for the algorithm. Furthermore, the convergence criteria of 10^{-8} for Problem (8) are satisfied in all but one case (S355J2+N 25 mm plate). In this case, the exit convergence criterion value was about 10^{-5} after 600 iterations. The plot of the objective function value at each iteration, Fig. 4b, indicates that the same level of error is reached regardless of the starting point. The reason is that the model parameters also converge to the same value for both SP1 and SP2, as shown in Fig. 4c that tracks the model parameters at each iteration. Therefore, the chosen starting points do not appear to be influential on the obtained solution point in this calibration procedure.

Validation

Data sets of uniaxial coupon tests conducted on samples from the flanges and web of an IPE300 profile of S355J2 steel are used as the *Validation* set for our proposed tensile-only calibration. The results of the validation are summarized in Table 5 via the $\bar{\varphi}$ metric. Values of the $\bar{\varphi}$ metric in this table are computed using all available load protocols for the IPE300 flange/web, and parameters that are either: (1) calibrated using the methodology in this paper using only the tensile test of the IPE300 flange or web data sets (tensile-only), or (2) calibrated using all available load protocols of other S355J2(+N) steel materials. For instance, the error computed across the entire IPE300 flange dataset using the parameters from the IPE300 tensile-only calibration is $\bar{\varphi} = 10.53$ %, while the error computed using the parameters from the S355J2+N (50 mm plate) dataset is $\bar{\varphi} = 11.25$ %. The implications of these results will be discussed shortly.

Figure 5 is provided to compare the level of fit between different options for selected tests from the IPE300 flange data set. Material model predictions in these figures are computed with the parameters from the VC 1-backstress model tensile-only calibration using the IPE300 flange ("Tensile"), and the VC 2-backstress model parameters calibrated to the S355J2 HEB500 flange data ("HEB500-Flange"). For the case shown in Fig. 5, the proposed tensile-only calibration leads to results that are in closer agreement with the test data regardless of the load protocol. Moreover, a stark contrast is apparent between the poor

results of the "naive" approach, where no information is used to guide the tensile-only calibration (see Fig. 1b/1d), and the reasonably good results shown in Fig. 5c when the proposed methodology is employed.

Updated Voce-Chaboche Model Results

Constraint Bounds

The same materials and methodology as discussed above for the VC model is applied to the UVC model to derive appropriate bounds of the model's material performance metrics. UVC material model parameters are provided in Table 6 for one and two backstresses, and the hardening metrics are summarized in Table 7. A summary of the metrics can also be viewed in graphical form in Fig. 3.

Many observations regarding the link between the calibration results and the physical material properties made for the VC model also apply to the UVC model. However, a quick review of the obtained metrics shows a significant dispersion in the ratios in the material metrics ρ_{iso}^{sat} and ρ_{D}^{sat} when only one backstress is included in the UVC model (see Figs. 3b and 3e). The later metric essentially measures the decay in isotropic hardening stress with respect to the other hardening components of the model, and the accuracy of this parameter is crucial to the UVC functioning as intended since it is the main differentiator with respect to the VC model. Furthermore, considering that these two metrics cannot be defined with precision, the initial hypothesis that these metrics are an intrinsic property of the material cannot be made with any degree of confidence when only one backstress is included in the UVC model. It follows, then, that it is pointless to pursue analyses with one backstress using the UVC model. This is not the case, however, for the two backstress condition, where ρ_{D}^{sat} and ρ_{iso}^{sat} are defined within a narrow CoV range.

Following the above argument, the recommended bounds used in this study to assess tensile-only calibrations for the UVC model are based solely on a two-backstress model. For the steels in question (S355J2(+N), A992 Gr. 50, and BCP325) these are: $1.8 \leq \rho_{yield}^{sat} \leq 2.1$, $0.25 \leq \rho_{iso}^{sat} \leq 0.30$, $13.0 \leq \rho_{\gamma_1 b} \leq 20.0$, $15.0 \leq \rho_{\gamma_1 \gamma_2} \leq 30.0$, and $0.2 \leq \rho_{D} \leq 0.3$.

Tensile-Only Calibration and Validation Results

In contrast with the VC model, UVC tensile-only parameters are not presented herein. The reason for this decision follows from the results in Table 8 for the validation of the UVC two-backstress model. This table indicates that, in terms of the error metric $\bar{\varphi}$, the performance of the tensile-only parameters is significantly worse than using the parameters from a different steel from a database derived with full load protocols (*i.e.*, using any of the two-backstress parameter sets from Table 6). For example, the error in the IPE300 web data set is around $\bar{\varphi} = 25$ % when the proposed tensile-only calibration procedure is used with the UVC model, while the error is around $\bar{\varphi} = 10$–18 % using the parameters calibrated from other data sets. Poor results of the UVC tensile-only calibration are apparent in Fig. 6: despite matching the tensile test, the other cyclic load protocols are not accurately represented by the model predictions. These results demonstrate that UVC tensile-only calibrations, even with two backstresses, are inadequate with the methodology and data presented herein, and should not be used when parameters from a material with a similar microstructure are available.

DISCUSSION

The methodology presented in this paper assumes a strong link between physical material response and the parameters used in its representation by a material constitutive model. This assumption is crucial in order to obtain accurate cyclic model responses by performing a constrained optimization with limited information (in this case a tensile-only test of a material sample). From the results presented in the previous section, it was shown that while precise performance metrics can be found for the material models under analysis (VC with one backstresses, and UVC with two backstresses), when these metrics are used in the constrained optimization with tensile-only test data, the results are not universally satisfactory. In fact, the poor performance of the UVC under these conditions leads to the inescapable conclusion that it should not be used for calibrations under limited information. This is not the case for the VC model– some nuances notwithstanding .

The results depicted in Table 4 for the VC show persistently that tensile-only calibrations with two backstresses underperform, in error-metric terms ($\bar{\varphi}$), the model with a single backstress. One key observation in this Table is that the second backstresses parameters are close to zero, meaning that the model response is close to a single-backstress condition. A probable cause for this result is the significant dispersion in the $\rho_{\gamma_1\gamma_2}$ performance metric in Table 3 and depicted in Fig. 3d, since it is the only metric that relates both backstresses. Furthermore, the consistency of the solutions, as measured by ξ_2 metric with respect to the parameters calibrated with all available load protocols, is significantly worst than the one-backstress case. Moreover, the results from the validation dataset shown in Table 5 show overwhelmingly that the tensile-only two-backstress VC, underperforms models with parameters unrelated to the specific sample, *i.e.* taken from another (Root) dataset. All-in-all, these findings seem to indicate that there just isn't enough information in a tensile test to accurately provide two-backstress VC model parameters and that, under conditions in which the modeler is faced with a single tensile-only test, it is preferable to use known database parameters rather than attempting to calibrate a two-backstress VC model. This conclusion, however, does not hold for the one-backstress VC model.

The one-backstress VC model performance, shown in Tables 4 and 5, suggests that error levels are typically smaller than the two-backstress tensile-only VC model. Moreover, in the validation cases the one-backstress model performs at error levels on or above par with respect to known two-backstress database parameters established with many more load protocols (the recommended VC calibrations strategy of de Castro e Sousa et al. (2020)). These results seem to indicate that a limited information calibration procedure with a one-backstress VC model is, in fact, a suitable approach to modeling material response when only monotonic test data is available. Indeed it could be said, also with respect to the UVC results, that the simplest model is the one that performs best under limited information conditions.

Why, then, should one find the possibility of using a single test result to calibrate a material model worthwhile? The main advantage of using the constrained optimization

procedure advocated in this paper, instead of using known database parameters, is that it diminishes the uncertainty related to the steel making process. Consider, for instance, using database parameters for S355J2 taken from an HEB500 flange and applying them to an S355J2 IPE300 flange. The results in Table 5 show that an error of $\bar{\varphi} = 16.91\%$ is obtained, whereas if the tensile-only IPE300 flange test is used, one obtains an error $\bar{\varphi} = 10.53\%$. This suggests that, although the materials are "*theoretically*" the same, variations in manufacturing conditions (*e.g.* differences between production batches or profile rolling schemes) can affect a material's cyclic response and that the methodology presented herein can mitigate this effect.

The facts above notwithstanding, if a modeler can have access to a material's cyclic response using multiple load protocols, the modeler should not hesitate in using them (de Castro e Sousa et al. 2020). The accuracy of the parameters obtained using multiple load protocols is substantially better than the alternatives (constrained optimization or established material databases). This can also be seen in Table 4, where mid-single-digit errors are obtained if a two-backstress solution with all available load protocols is used. Moreover, it should be noted that, although satisfactory results are obtained using the one-backstress VC model tensile-only method, the values of $\xi_2 > 5\%$ in Table 4 indicate that the parameters are inconsistent with those obtainable from more protocols – *c.f.* de Castro e Sousa et al. (2020) for details on the 5% bound. In other words, the proposed method is acceptable **only** in situations where limited information is available on the material at hand, but it is not without its shortcomings.

Another disadvantage of this methodology is the fact that best-fit is only achieved with a one-backstress solution for the VC model. The feature restricts the possible shapes of the hardening material, which in certain applications may reveal crucial. Here, care should be taken on the range of plastic strains to which the model is to be applied. For instance, hardening slopes play a significant role in localization problems and, as such, this approach is likely not suitable in studying cases like ultra low cycle fatigue of materials where significant

plastic strains ranges coupled with damage occurs. It should be stated, in fact, that the most suitable cases to use in this approach would be cases where nominal strains (as opposed to strain riser regions, such as sharp geometry changes or welds) are fairly bounded (between -5/+5 % plastic strains, the range of most cyclic calibration tests).

Lastly, it should be noted that the best-fit constrained optimization method presented herein is geared toward obtaining better cyclic material properties than otherwise obtained with a tensile test or from existing databases, which may not directly translate itself to a "best-fit" component behavior. The material will be better characterized (as shown above), but how this relates to a better hysteretic response on the component side is a different issue. Component behavior depends not only on material characteristics, but also on how these interact with other features like its slenderness, geometric imperfections or residual stresses and demand histories. As such, one can only point out to the component modeler that some care should be taken with regards to the sensitivity of the component response to material parameters, because cases can arise where different failure modes can be triggered as a function of the material response (Hartloper et al. 2019a).

CONCLUSIONS

This paper presented a methodology to obtain material model parameters under limited information conditions. The models discussed herein are the Voce-Chaboche (VC) and an Updated Voce-Chaboche (UVC) in the context of structural steel applications. Limited information conditions can arise when one intends to study the behavior of steel structures under large amplitude cyclic loading, but knowledge of the employed steel material is restricted to a single tensile test. A procedure is proposed herein that allows the calibration of material parameters taking into account its cyclic properties with a single monotonic test using a constrained optimization scheme. This procedure has been incorporated into the open-source Python library, `RESSPyLab` (de Castro e Sousa et al. 2019), which is made publicly available. The following conclusions can be made from this work:

- The definition of adequate material cyclic-performance metrics is an essential part

in the constrained optimization procedure. Metrics are proposed herein that relate typical ratios of isotropic to kinematic hardening and their rates in order to inform the constrained optimization procedure;

- The number of backstresses used in the kinematic part of the models plays a significant role in the accuracy of tensile-only parameter estimates;

- The UVC model does not provide satisfactory results in parameter estimates in the tensile-only constrained optimization, regardless of the number of backstresses employed;

- The VC model with two backstresses does not provide satisfactory estimates of material response for tensile-only calibrations with the constraints presented herein. More data can however motivate different constraints;

- The VC model with one backstress, however, yields satisfactory results and is the recommended material model if a modeler is faced with a situation where tensile-only data is available.

It should be underscored that this methodology is a best-fit approximation in limited information cases. Whenever possible, material testing taking into account multiple load protocols should, nevertheless, be used.

DATA AVAILABILITY

Some or all data, models, or code generated or used during the study are available in a repository or online in accordance with funder data retention policies (de Castro e Sousa et al. 2019).

ACKNOWLEDGMENTS

The authors recognize and are grateful for the financial support of this study by the Nippon Steel Corporation, internal grants from École Polytechnique Fédérale de Lausanne

(EPFL), as well as an exploratory grant from EPFL's School of Environmental, Architectural and Civil Engineering, and the Swiss National Science Foundation (Project No. 200021_188476). Any opinions, findings, and conclusions or recommendations expressed in this paper are those of the authors and do not necessarily reflect the views of sponsors.

REFERENCES

Araújo, M., Macedo, L., and Castro, J. M. (2017). "Evaluation of the rotation capacity limits of steel members defined in EC8-3." *Journal of Constructional Steel Research*, 135, 11–29.

Armstrong, P. and Fredrick, C. (1966). "A Mathematical Representation of the Multiaxial Bauschinger Effect." *Report No. RD/B/N 731*, Central Electricity Generating Board.

ASCE (2017). "ASCE 41-17 - Seismic Evaluation and retrofit of existing buildings." American Society of Civil Engineers (ASCE).

ASTM (2013). *E8/E8M - 13a - Standard Test Methods for Tension Testing of Metallic Materials 1*. ASTM International, West Conshohocken, PA, USA.

ASTM (2016). "Standard Specification for General Requirements for Rolled Structural Steel Bars, Plates, Shapes, and Sheet Piling." *A6/A6M-16a*, ASTM International, West Conshohocken, PA, USA.

ASTM (2018). "Standard Terminology Relating to Steel, Stainless Steel, Related Alloys, and Ferroalloys." *A941-18*, ASTM International, West Conshohocken, PA, USA.

Bouaziz, O., Aouafi, A., and Allain, S. (2008). "Effect of grain refinement on the mechanical behaviour of ferritic steels: Evolution of isotropic hardening and kinematic hardening." *Materials Science Forum*, 584-586 PA, 605–609.

Byrd, R. H., Hribar, M. E., and Nocedal, J. (1999). "An Interior Point Algorithm for Large-Scale Nonlinear Programming." *SIAM Journal on Optimization*, 9(4), 877–900.

CEN (2001). "EN 10002-1:2001 - Metallic materials Tensile testing Part 1: method of test at ambient temperature." European Comission for Standardization (CEN).

CEN (2005). "EN 1998-3: Eurocode 8: Design of structures for earthquake resistance - Part

672 3: Assessement and retrofitting of buildings." European Comission for Standardization
673 (CEN).
674 CEN (2005). "Hot rolled products of structural steels - Part 2: Technical delivery conditions
675 for non-alloy structural steels." *NF EN 10025-2*, European Comission for Standardization
676 (CEN), Brussels, Belgium.
677 CEN (2019a). "Hot rolled products of structural steels - Part 3: Technical delivery conditions
678 for normalized/normalized rolled weldable fine grain structural steels." *NF EN 10025-3*,
679 European Comission for Standardization (CEN), Brussels, Belgium.
680 CEN (2019b). "Hot rolled products of structural steels - Part 6: Technical delivery conditions
681 for flat products of high yield strength structural steels in the quenched and tempered
682 condition." *NF EN 10025-6*, European Comission for Standardization (CEN), Brussels,
683 Belgium.
684 Chaboche, J., Dang Van, K., and Codier, G. (1979). "Modelization of the Strain Memory
685 Effect on the Cyclic Hardening of 316 Stainless Steel." *Structural mechanics in reactor*
686 *technology - SMiRT 5*, L11.
687 Cooke, R. J. and Kanvinde, A. M. (2015). "Constitutive parameter calibration for structural
688 steel: Non-uniqueness and loss of accuracy." *Journal of Constructional Steel Research*,
689 114, 394–404.
690 de Castro e Sousa, A., Hartloper, A. R., and Lignos, D. G. (2019). "RESSPyLab version 1.0
691 - Python tools for structural steel research, <https://pypi.org/project/RESSPyLab/>.
692 de Castro e Sousa, A., Suzuki, Y., and Lignos, D. (2020). "Consistency in Solving the
693 Inverse Problem of the Voce-Chaboche Constitutive Model for Plastic Straining." *Journal*
694 *of Engineering Mechanics*, 146(9), 1–16.
695 Elkady, A. and Lignos, D. G. (2018). "Improved Seismic Design and Nonlinear Modeling
696 Recommendations for Wide-Flange Steel Columns." *Journal of Structural Engineering*,
697 144(9), 04018162.
698 Fell, B. V., Kanvinde, A. M., Deierlein, G. G., and Myers, A. T. (2009). "Experimental

699 investigation of inelastic cyclic buckling and fracture of steel braces." *Journal of Structural*
700 *Engineering*, 135(1), 19–32.

701 Grigoriou, V. and Lignos, D. G. (2017). "Characterization of the cyclic hardening properties
702 of european steels." *Report No. (unpublished)*, EPFL - RESSLab.

703 Hartloper, A., de Castro e Sousa, A., and Lignos, D. G. (2019a). "Sensitivity of Simu-
704 lated Steel Column Instabilities to Plasticity Model Assumptions." *Proceedings of the*
705 *12th Canadian Conference on Earthquake Engineering*, Quebec City, QC, Canada, 8.

706 Hartloper, A. R., de Castro e Sousa, A., and Lignos, D. G. (2019b). "A Nonlinear
707 Isotropic/Kinematic Hardening Model for Materials with Discontinuous Yielding." *Re-*
708 *port No. 271062*, Resilient Steel Structures Laboratory, École Polytechnique Fédérale de
709 Lausanne (EPFL), Lausanne, Switzerland.

710 Hartloper, A. R., de Castro e Sousa, A., and Lignos, D. G. (2020). "Constitutive Modeling
711 of Structural Steels: A Nonlinear Isotropic/Kinematic Hardening Material Model and its
712 Calibration." *Journal of Structural Engineering*, (under review).

713 Lubliner, J. (2008). *Plasticity Theory*. Dover Publications, Mineola, N.Y., U.S.A.

714 Suzuki, T., Yoshida, Y., Shimura, Y., Suzuki, Y., Kubota, S., and Nagata, M. (2008).
715 "Development of Building Structural Steel with High Yield Ratio and High Yield Point
716 Leading to Innovative Steel Structural System." *Report No. 97*, Nippon Steel, Tokyo,
717 Japan.

718 Suzuki, Y. (2018). "Earthquake-induced collapse of steel moment resisting frames with con-
719 ventional and high performance steel columns." Ph.D. thesis, McGill University, Montreal,
720 QC, Canada.

721 Virtanen, P., Gommers, R., Oliphant, T. E., Haberland, M., Reddy, T., Cournapeau, D.,
722 Burovski, E., Peterson, P., Weckesser, W., Bright, J., van der Walt, S. J., Brett, M.,
723 Wilson, J., Millman, K. J., Mayorov, N., Nelson, A. R. J., Jones, E., Kern, R., Larson,
724 E., Carey, C. J., Polat, İ., Feng, Y., Moore, E. W., VanderPlas, J., Laxalde, D., Perktold,
725 J., Cimrman, R., Henriksen, I., Quintero, E. A., Harris, C. R., Archibald, A. M., Ribeiro,

726 A. H., Pedregosa, F., van Mulbregt, P., and SciPy 1.0 Contributors (2020). "SciPy 1.0:
727 Fundamental Algorithms for Scientific Computing in Python." *Nature Methods*, 17, 261–
728 272.
729 Voce, E. (1948). "The relationship between stress and strain for homogenous deformation."
730 *Journal of Institute of Metals*, 74, 537–562.

NOTATION

The following symbols are used in this paper:

a = isotropic saturation rate parameter associated with D_∞;

b = isotropic saturation rate parameter associated with Q_∞;

C_k = kinematic stress parameter for the k-th backstress;

c = constant in hardening metric constraint;

D_∞ = isotropic differential stress at saturation for discontinuous yielding;

E = Young's modulus;

E_{total} = total normalized strain energy in stress-strain data;

$f(\boldsymbol{x})$ = objective function in minimization problem with vector variable $\boldsymbol{x}$;

g = constraint on hardening metric;

Q_∞ = isotropic differential stress at saturation;

γ_k = kinematic saturation rate parameter for the k-th backstress;

ε = uniaxial true strain;

ε^* = error-metric strain;

$\dot{\varepsilon}^p_{eq}$ = equivalent plastic strain;

ξ_2 = consistency distance metric;

ρ = constitutive model hardening metric;

σ = uniaxial true stress;

$\sigma_{y,0}$ = initial yield stress;

φ = error function;

$\bar{\varphi}$ = normalized error function;

ϕ^{VM} = Von Mises yield criterion;

$\boldsymbol{\nabla}_x f(\boldsymbol{x})$ = gradient of function f with respect to vector variable $\boldsymbol{x}$;

$\boldsymbol{\nabla}_{xx} f(\boldsymbol{x})$ = hessian of function f with respect to vector variable $\boldsymbol{x}$;

List of Tables

TABLE 1: Overview of the Root material database.

ID	Material	Source	Tested By[a]	Load Protocols	$f_{y,n}$[b] [MPa]	$f_{u,n}$[c] [MPa]
1	S355J2+N	50 mm plate	1	1–10	355	470–630
2	S355J2+N	25 mm plate	1	1–10	355	470–630
3	S355J2	HEB500 flange	3	1,2,5,6,9	355	470–630
4	S355J2	HEB500 web	3	1,1–3,5–9	355	470–630
5	S460NL	25 mm plate	1	1,3–7,9,10	440	540–720
6	S690QL	25 mm plate	1	1,3–7,9,10	690	770–940
7	A992 Gr.50	W14X82 web	2	1,2,5,6,9	345	450[d]
8	A992 Gr.50	W14X82 flange	2	1,2,5,6,9	345	450[d]
9	A500 Gr.B	HSS305X16	2	1,2,5,6,9	315	400[d]
10	BCP325	22 mm plate	2	1,2,5,6,9	325	490–610
11	BCR295	HSS350X22	2	1,2,5,6,9	295	400–550
12	HYP400	27 mm plate	2	1,2,5,6,9	400	490–640

[a] 1: Grigoriou and Lignos (2017), 2: Suzuki (2018), 3: Hartloper et al. (2020).

[b]: nominal yield stress, [c]: nominal tensile stress, [d]: minimum value.

TABLE 2: Voce-Chaboche material model parameters with one and two backstresses obtained using the full data sets.

ID	$\bar{\varphi}$ [%]	E [GPa]	$\sigma_{y,0}$ [MPa]	Q_∞	b [MPa]	C_1	γ_1	C_2 [MPa]	γ_2
1	8.21	177.54	296.62	123.26	7.17	6501.83	27.90	-	-
	6.31	184.98	270.96	107.22	5.97	14327.30	115.12	1771.06	7.56
2	8.49	182.11	285.67	125.79	11.80	6801.09	29.78	-	-
	6.57	191.52	265.29	104.45	11.63	12997.99	99.51	1560.41	7.35
3	6.02	186.13	272.57	132.55	9.10	3738.39	28.95	-	-
	4.63	191.85	245.50	119.77	8.67	14019.86	205.39	1247.05	4.45
4	7.38	193.82	275.65	104.97	14.29	8437.43	62.41	-	-
	6.86	200.39	265.46	103.29	11.18	11996.11	104.79	627.33	1.14
5	8.02	172.85	376.44	106.09	11.08	6857.43	23.44	-	-
	6.18	185.86	358.93	68.04	10.02	14202.40	104.22	2259.11	8.01
6	7.56	184.88	607.47	0.50	0.58	15648.17	60.98	-	-
	7.29	184.70	602.64	0.48	0.55	16107.81	78.81	937.51	6.32
7	7.78	194.55	328.83	101.76	16.73	5159.90	38.80	-	-
	6.23	207.32	299.86	88.30	13.96	14878.98	166.00	1424.51	8.57
8	7.69	178.64	324.68	127.20	11.89	3943.98	30.59	-	-
	5.75	189.95	292.75	110.54	9.71	15142.58	170.54	1117.53	5.86
9	7.72	180.57	321.68	36.64	0.94	3995.53	24.59	-	-
	5.43	191.39	286.87	24.08	0.84	11934.29	160.01	1585.62	7.71
10	6.67	173.87	325.05	103.34	8.75	5945.26	32.19	-	-
	4.88	177.92	306.09	94.16	5.81	11613.11	122.00	1744.03	8.29
11	7.75	173.46	355.97	0.56	0.60	5135.19	44.95	-	-
	6.24	177.88	329.13	0.57	0.61	12773.06	196.86	1746.22	11.96
12	7.02	187.13	401.29	44.20	9.64	5758.71	38.19	-	-
	5.22	189.35	376.22	29.12	6.41	13711.66	139.70	1147.15	4.59

TABLE 3: Voce-Chaboche hardening metrics with one and two backstresses obtained using the full data sets.

	One Backstress			Two Backstresses			
ID	ρ_{yield}^{sat}	ρ_{iso}^{sat}	$\rho_{\gamma_1 b}$	ρ_{yield}^{sat}	ρ_{iso}^{sat}	$\rho_{\gamma_1 b}$	$\rho_{\gamma_1 \gamma_2}$
1	2.20	0.35	3.89	2.72	0.23	19.27	15.22
2	2.24	0.36	2.52	2.69	0.23	8.56	13.55
3	1.96	0.51	3.18	2.91	0.26	23.70	46.13
4	1.87	0.44	4.37	3.90	0.13	9.37	92.16
7	1.71	0.43	2.32	2.15	0.26	11.89	19.37
8	1.79	0.50	2.57	2.33	0.28	17.56	29.12
10	1.89	0.36	3.68	2.31	0.24	21.00	14.72
Avg.	1.95	0.42	3.22	2.72	0.23	15.91	32.90
StD.	0.19	0.06	0.73	0.54	0.05	5.52	26.46
CoV.[%]	9.49	14.76	22.61	20.05	19.44	34.72	80.44

TABLE 4: Voce-Chaboche tensile test only calibration with one and two backstresses using the NITRO algorithm and SP1 for mild steels.

ID	$\bar{\varphi}$ [%]	ξ_2 [%]	E [GPa]	$\sigma_{y,0}$ [MPa]	Q_∞ [MPa]	b	C_1 [MPa]	γ_1	C_2 [MPa]	γ_2
1	12.4	13.5	206.38	298.28	201.10	7.10	4692.07	23.07	-	-
	14.31	37.0	199.38	308.79	60.68	1.79	5183.37	15.21	0.01	1.17
2	12.4	14.4	200.40	299.99	193.89	8.15	4861.80	25.00	-	-
	13.65	44.0	200.87	311.37	82.02	1.96	5380.87	16.67	0.04	1.28
3	9.5	10.9	220.12	300.02	157.51	3.07	2018.60	6.90	-	-
	18.05	20.9	200.00	289.05	55.60	0.41	3081.98	9.85	0.16	0.76
4	11.5	7.5	204.86	290.20	118.20	6.23	3078.12	14.02	-	-
	19.01	37.5	200.00	291.16	77.46	1.09	3666.21	12.24	0.69	0.94
7	8.68	4.6	200.95	356.51	104.04	6.90	2999.91	15.53	-	-
	14.97	7.4	200.00	357.10	60.84	0.54	3619.24	13.25	0.91	1.02
8	10.1	9.3	200.15	339.64	114.86	5.61	2690.49	12.61	-	-
	19.45	13.0	200.00	331.53	78.09	0.51	3656.42	12.51	0.81	0.96
10	10.5	12.1	212.62	353.76	114.24	6.21	2965.99	13.98	-	-
	14.30	10.2	200.00	352.67	81.40	0.51	3662.68	12.33	1.33	0.95

TABLE 5: Results from the validation of the tensile test only calibration methodology with one and two backstresses, using the VC model for mild steels.

Calibration Data Set	Material	Load Protocols	Model	IPE300 flange $\bar{\varphi}$,[%]	IPE300 web $\bar{\varphi}$,[%]
Validation	S355J2 (IPE300 flange)	Tensile only	VC, 1bk	10.53	-
Validation	S355J2 (IPE300 web)	Tensile only	VC, 1bk	-	11.82
Validation	S355J2 (IPE300 flange)	Tensile only	VC, 2bk	18.31	-
Validation	S355J2 (IPE300 web)	Tensile only	VC, 2bk	-	19.92
Validation	S355J2 (IPE300 flange)	All available	VC, 2bk	5.46	6.94
Validation	S355J2 (IPE300 web)	All available	VC, 2bk	6.03	6.26
Root	S355J2+N (50 mm plate)	All available	VC, 2bk	11.25	11.86
Root	S355J2+N (25 mm plate)	All available	VC, 2bk	10.71	11.50
Root	S355J2 (HEB500 flange)	All available	VC, 2bk	16.91	18.36
Root	S355J2 (HEB500 web)	All available	VC, 2bk	11.99	13.64

TABLE 6: Updated Voce-Chaboche full data set calibration with one and two backstresses for mild steels.

ID	$\bar{\varphi}$ [%]	E [GPa]	$\sigma_{y,0}$ [MPa]	Q_∞ [MPa]	b	D_∞ [MPa]	a	C_1 [MPa]	γ_1	C_2 [MPa]	γ_2
1	8.18	177.51	327.15	128.25	7.86	37.28	203.33	6572.34	28.32	-	-
	6.33	197.41	338.8	134.34	14.71	133.75	229.25	26242.00	199.04	2445.30	11.66
2	8.43	182.96	330.42	146.77	13.72	67.20	133.57	6962.12	30.65	-	-
	6.53	185.97	332.18	120.48	8.14	93.15	261.75	21102.00	173.60	2300.60	10.42
3	5.81	186.17	304.96	153.96	12.13	59.91	98.68	4044.49	32.44	-	-
	3.96	192.13	315.04	138.01	11.36	96.16	223.66	18587.84	257.31	1351.98	6.52
4	7.00	193.91	341.22	454.07	34.70	419.75	56.92	8907.58	66.38	-	-
	6.61	199.68	334.94	139.32	14.07	120.33	274.73	28528.03	315.17	2569.46	24.68
7	7.43	194.62	376.35	623.86	38.46	574.87	51.64	5690.09	44.29	-	-
	5.21	210.72	378.83	122.63	19.74	143.49	248.14	31638.00	277.32	1548.60	9.04
8	7.53	178.75	360.64	195.99	20.52	113.60	74.36	4425.80	36.83	-	-
	4.76	191.02	373.72	141.47	15.20	135.95	211.16	25621.00	235.12	942.18	3.16
10	6.51	173.95	360.85	123.00	12.50	60.74	127.27	6193.34	34.44	-	-
	3.89	178.61	368.03	112.25	10.78	105.95	221.92	20104.00	200.43	2203.00	11.76

TABLE 7: Metrics for the Updated Voce-Chaboche full data set calibration with one and two backstresses.

	One Backstress				Two Backstresses				
ID	ρ^{sat}_{yield}	ρ^{sat}_{iso}	$\rho^{sat}_{\gamma_1 b}$	ρ^{sat}_{D}	ρ^{sat}_{yield}	ρ^{sat}_{iso}	$\rho^{sat}_{\gamma_1 b}$	ρ^{sat}_{D}	ρ_{γ_1/γ_2}
1	1.99	0.36	3.60	0.10	2.11	0.26	21.33	0.20	16.67
2	1.93	0.39	2.23	0.18	2.01	0.28	13.53	0.28	17.08
3	1.72	0.55	2.68	0.22	2.02	0.33	22.65	0.23	39.49
4	1.49	0.77	1.91	0.71	1.64	0.42	22.39	0.36	12.77
7	1.47	0.83	1.15	0.76	1.70	0.30	14.05	0.35	30.66
8	1.56	0.62	1.80	0.36	2.10	0.26	15.47	0.25	74.44
10	1.67	0.41	2.76	0.20	1.80	0.28	18.60	0.26	17.05
Avg.	1.69	0.56	2.30	0.36	1.91	0.30	18.29	0.28	29.74
StD.	0.19	0.17	0.73	0.25	0.18	0.05	3.66	0.06	20.26
CoV. [%]	11.28	31.00	31.87	68.39	9.43	17.20	20.01	20.04	68.14

TABLE 8: Results from the validation of the tensile test only calibration methodology with two backstresses for the UVC model.

Calibration Data Set	Material	Load Protocols	Model	IPE300 flange $\bar{\varphi}$,[%]	IPE300 web $\bar{\varphi}$,[%]
Validation	S355J2 (IPE300 flange)	Tensile only	UVC, 2bk	19.80	-
Validation	S355J2 (IPE300 web)	Tensile only	UVC, 2bk	-	24.69
Validation	S355J2 (IPE300 flange)	All available	UVC, 2bk	4.94	6.35
Validation	S355J2 (IPE300 web)	All available	UVC, 2bk	5.59	5.42
Root	S355J2+N (50 mm plate)	All available	UVC, 2bk	10.86	11.31
Root	S355J2+N (25 mm plate)	All available	UVC, 2bk	10.19	10.69
Root	S355J2 (HEB500 flange)	All available	UVC, 2bk	16.42	17.86
Root	S355J2 (HEB500 web)	All available	UVC, 2bk	10.40	12.19

List of Figures

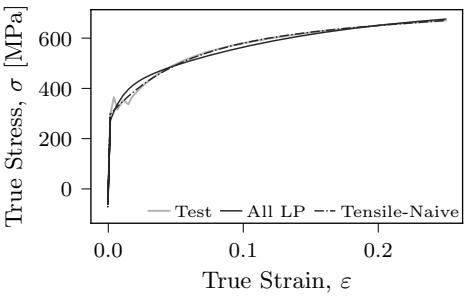

(a) S355J2+N, tensile (Load Protocol 1)

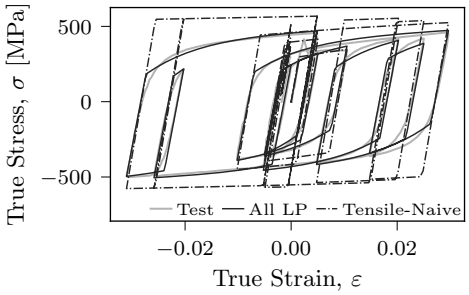

(b) S355J2+N, variable amplitude (Load Protocol 9)

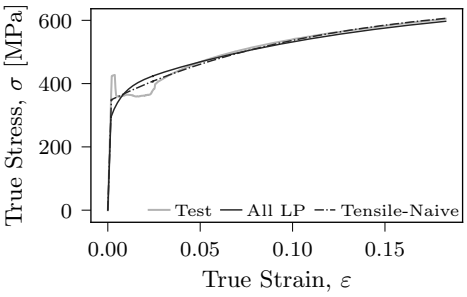

(c) A992Gr.50, tensile (Load Protocol 1)

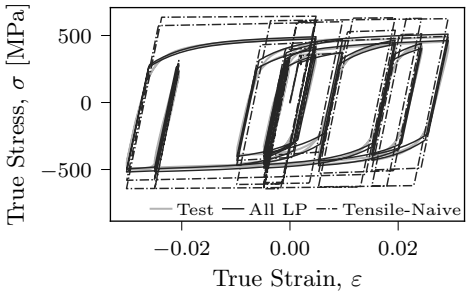

(d) A992Gr.50, variable amplitude (Load Protocol 9)

FIG. 1: Comparison of stress-strain using the S355J2+N 50 mm plate and A992 Gr. 50 W14X82 flange data sets: test data (Test); VC model 2 backstresses, all load protocols used in calibration (All LP); and naive calibration using only a tensile test (Tensile-Naive).

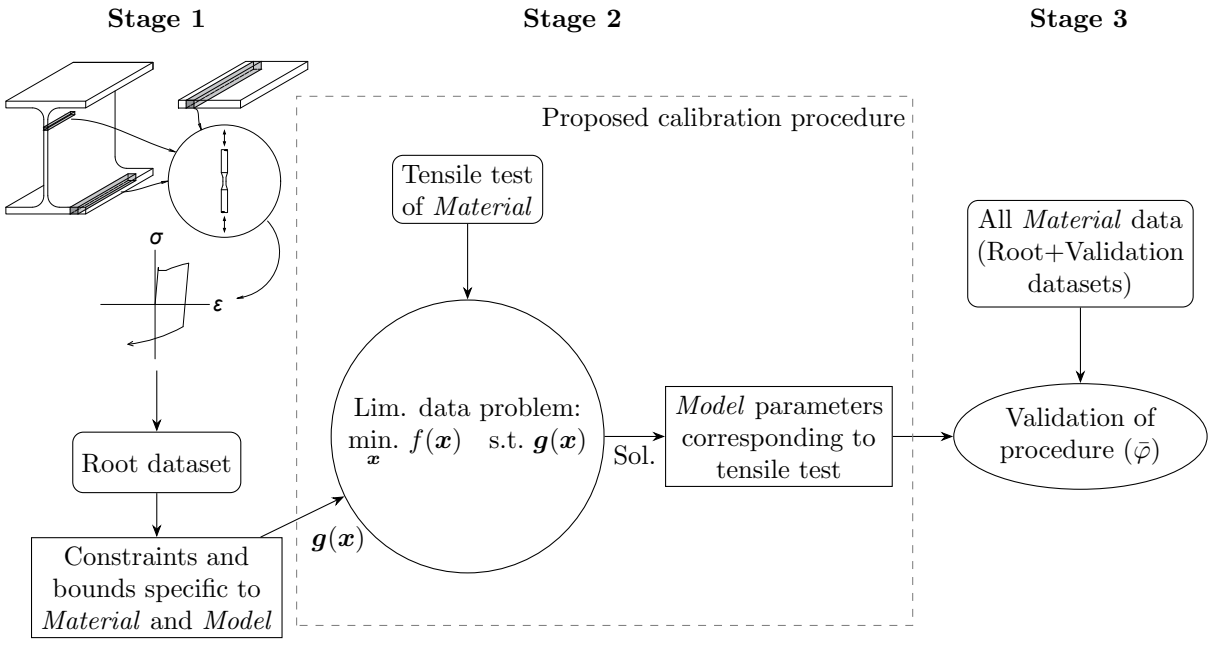

FIG. 2: Workflow of proposed methodology applied to structural steel materials.

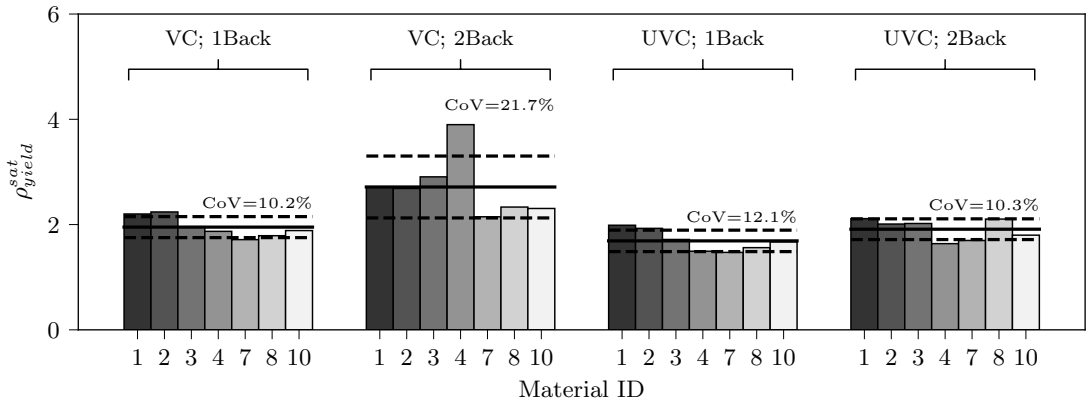

(a)

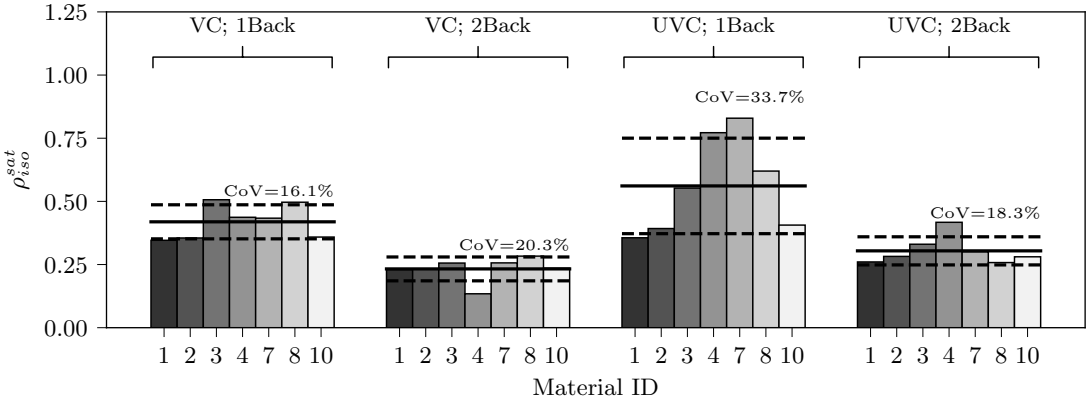

(b)

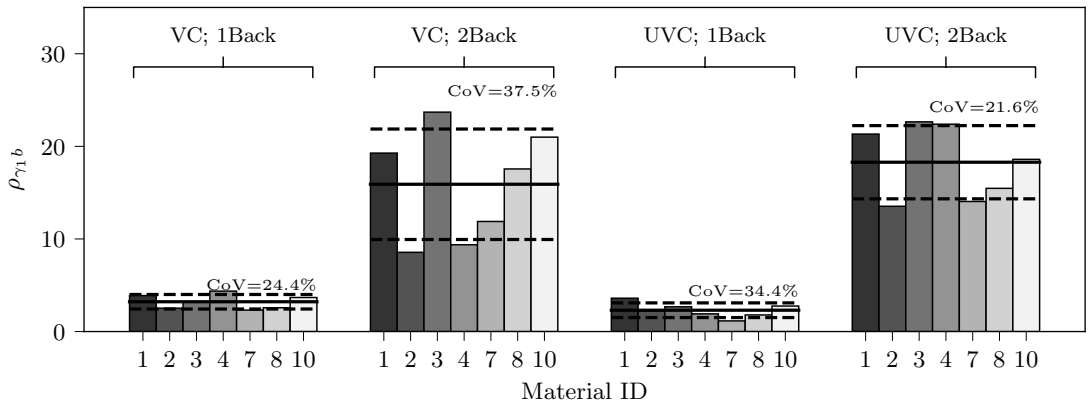

(c)

FIG. 3: Relevant model metrics for $\sigma_y \approx 355$ MPa materials based on parameters calibrated with all available load protocols.

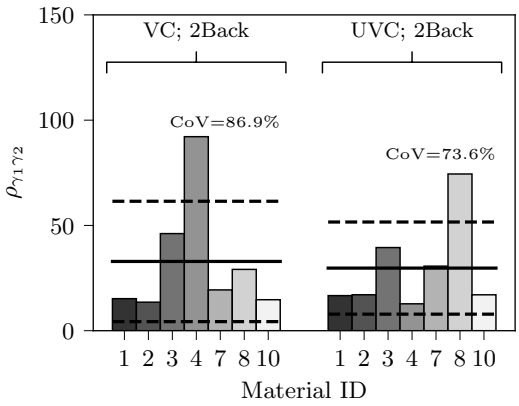

(d) (cont.)

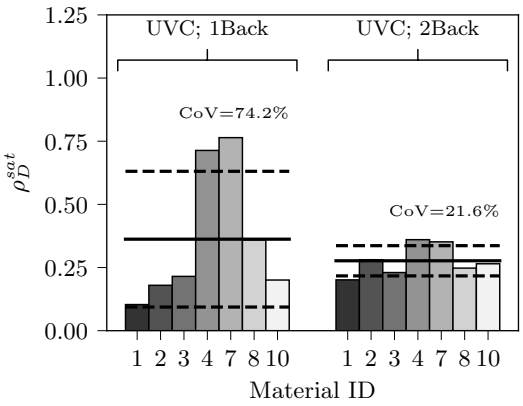

(e)

FIG. 3: Relevant model metrics for $\sigma_y \approx 355$ MPa materials based on parameters calibrated with all available load protocols. (Cont.)

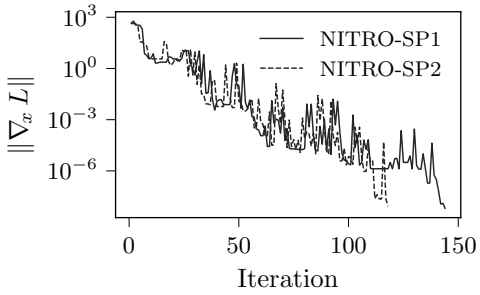

(a) Convergence criteria

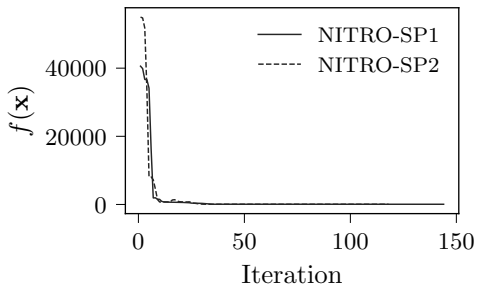

(b) Objective function

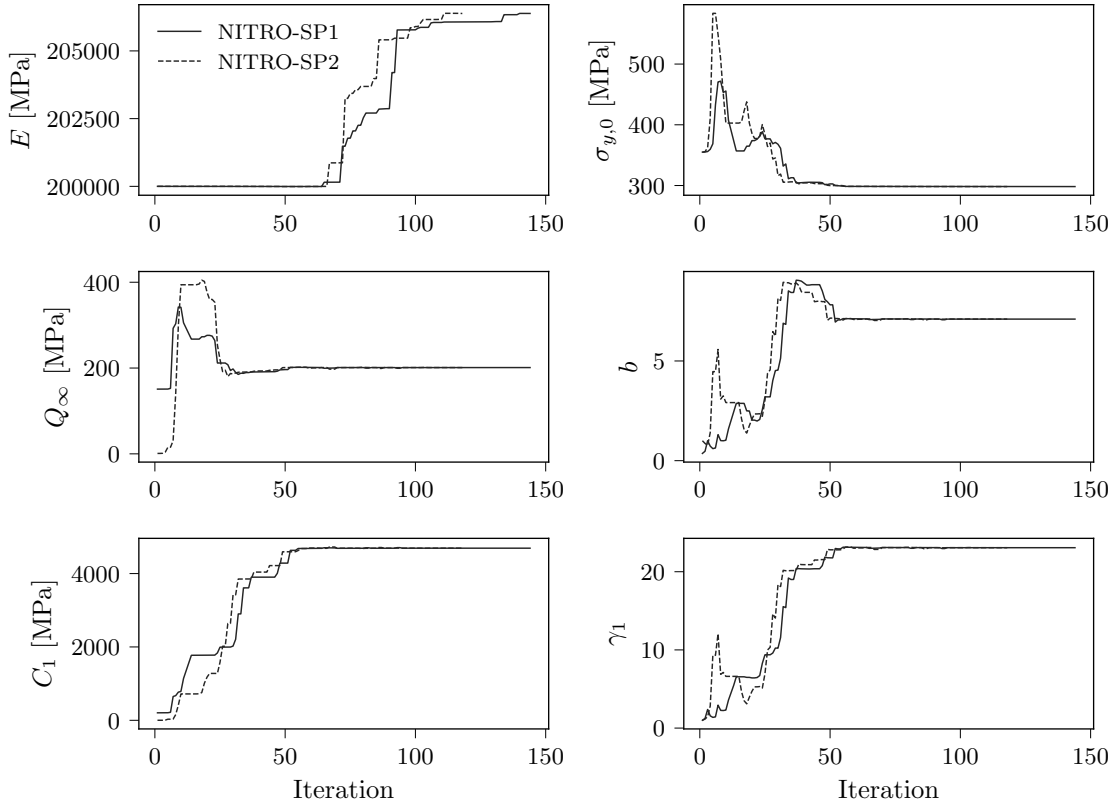

(c) Parameter values

FIG. 4: Evolution of the constrained optimization solution based on the different starting points using the S355J2+N 50 mm data set.

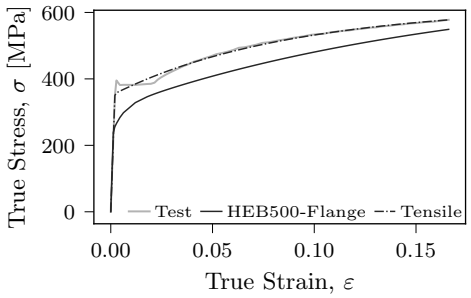

(a) VC, Load Protocol 1

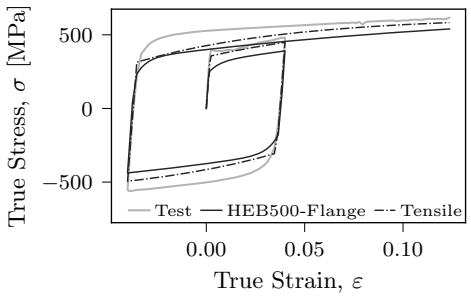

(b) VC, Load Protocol 3

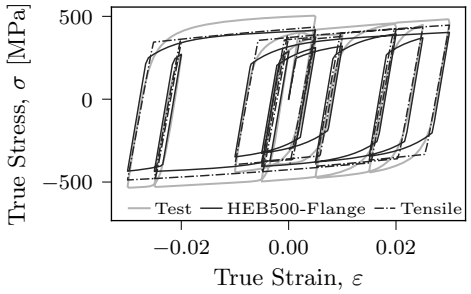

(c) VC, Load Protocol 9

FIG. 5: Comparison of stress-strain using the S355J2 IPE300 flange data set: test data (Test), VC 2Back Root dataset calibration (HEB500-Flange), and proposed tensile-only calibration with the VC model (Tensile).

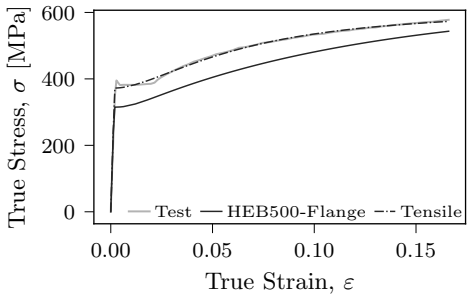

(a) UVC, Load Protocol 1

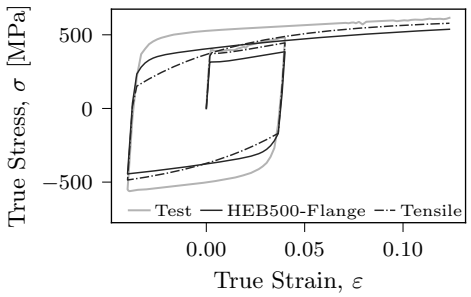

(b) UVC, Load Protocol 3

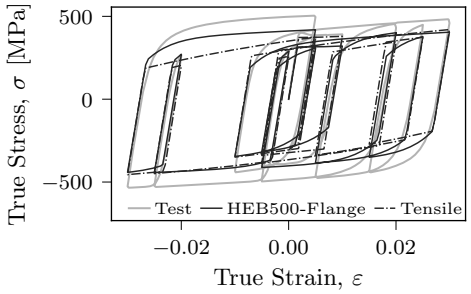

(c) UVC, Load Protocol 9

FIG. 6: Comparison of stress-strain using the S355J2 IPE300 flange data set: test data (Test), UVC 2Back Root dataset calibration (HEB500-Flange), and proposed tensile-only calibration with the UVC model (Tensile).